

The nature of the Roberge-Weiss Transition in $N_f = 2$ QCD with Wilson Fermions on $N_\tau = 6$ lattices

Francesca Cuteri¹, Christopher Czaban^{*1,2}, Owe Philipsen^{1,2}, Christopher Pinke¹,
Alessandro Sciarra¹

¹*Institut für Theoretische Physik - Johann Wolfgang Goethe-Universität
Max-von-Laue-Str. 1, 60438 Frankfurt am Main*

²*John von Neumann Institute for Computing (NIC)
GSI, Planckstr. 1, 64291 Darmstadt, Germany*

*E-mail: cuteri, czaban, philipsen, pinke, sciarra
@th.physik.uni-frankfurt.de*

The finite temperature chiral and deconfinement phase transitions at zero density for light and heavy quarks, respectively, have analytic continuations to imaginary chemical potential. At some critical imaginary chemical potential, they meet the Roberge-Weiss transition between adjacent $Z(3)$ sectors. For light and heavy quarks, where the chiral and deconfinement transitions are first order, the transition lines meet in a triple point. For intermediate masses chiral or deconfinement transitions are crossover and the Roberge-Weiss transition ends in a second order point. At the boundary between these regimes the junction is a tricritical point, as shown in studies with $N_f = 2, 3$ flavors of staggered and Wilson quarks on $N_\tau = 4$ lattices. Employing finite size scaling we investigate the nature of this point as a function of quark mass for $N_f = 2$ flavors of Wilson fermions with a temporal lattice extent of $N_\tau = 6$. In particular we are interested in the change of the location of tricritical points compared to our earlier study on $N_\tau = 4$.

*The 33rd International Symposium on Lattice Field Theory
14 -18 July 2015
Kobe International Conference Center, Kobe, Japan*

*Speaker.

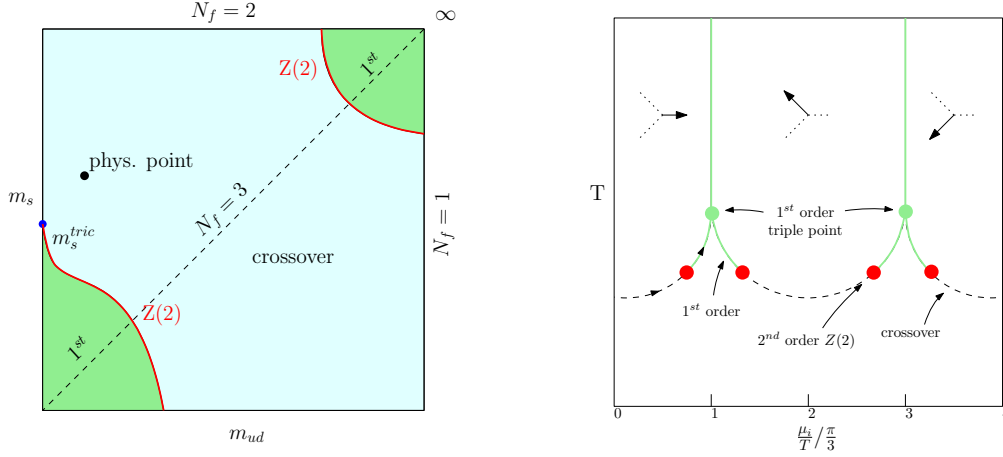


Figure 1: (Left) Columbia plot at $\mu = 0$. (Right) Schematic phase diagram of QCD at imaginary chemical potential. Illustrated is the change of the nature of the chiral/deconf. transition for a particular combination of $m_{u,d}$, m_s .

1. Introduction

The QCD phase diagram confronts us with many open questions. An interesting one addresses the nature of the phase transition in the two flavor chiral limit at zero chemical potential which has yet to be determined (see Fig. 1) and goes along with important insights about the physical QCD phase diagram. Symmetry arguments rule out an analytic crossover leaving either a first order or a second order phase transition. In the past many attempts have been undertaken to map out this region with standard simulation techniques resulting in many contradicting [1, 2, 3] lattice results between different fermion discretizations (e.g. staggered and Wilson). Closely related to this issue are the high computational costs arising due to low quark masses. A different approach to simulating at increasingly smaller quark masses is to choose a purely imaginary chemical potential (proposed in [4]) for which hybrid Monte Carlo (HMC) algorithms can be applied due to the absence of the sign problem. For purely imaginary chemical potential the center symmetry is extended to the periodic Roberge-Weiss symmetry [5]. In this region QCD exhibits a rich phase structure and features properties that can be used to impose constraints on the phase diagram at real chemical potential to a certain extent. In former studies on $N_\tau = 4$ lattices [6] we investigated these properties for $N_f = 2$ flavors of Wilson fermions by mapping out tricritical points at a critical value of μ_i . The present work presents our results of progressing to a finer lattice with an temporal extent of $N_\tau = 6$, taking a step towards the continuum.

2. The QCD phase structure for imaginary μ

For purely imaginary chemical potential the symmetries of the QCD partition function are reflection in μ and periodicity [5]

$$Z(\mu) = Z(-\mu), \quad Z\left(\frac{\mu}{T}\right) = Z\left(\frac{\mu}{T} + i\frac{2\pi n}{3}\right). \quad (2.1)$$

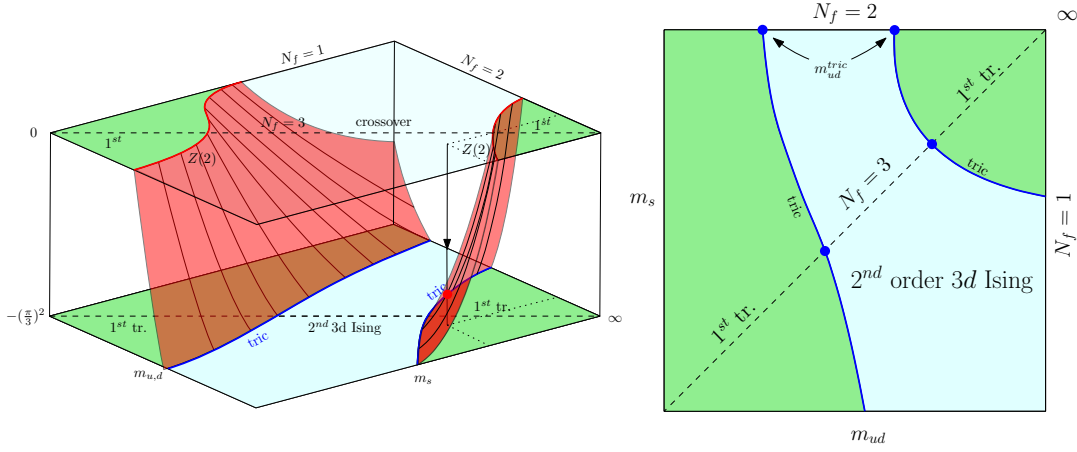


Figure 2: (Left) The Columbia plot with $(\mu/T)^2$ as an additional parameter. The $Z(2)$ critical lines became surfaces terminating in tricritical lines at critical values (μ_i^c/T) . (Right) A Stripe of the left figure at (μ_i^c/T) .

As shown in Fig. 1 there are center sectors separated by discrete values

$$\left(\frac{\mu_i}{T}\right)_c = \frac{\pi}{3}(2n+1), \quad n \in \mathbb{Z}. \quad (2.2)$$

Above a critical temperature T_c the Roberge-Weiss (RW) transition between the $Z(3)$ center sectors is of first order, represented by the vertical lines, whereas it is a mere crossover below T_c [5, 7, 8]. Physical observables are not sensitive to the sectors though it is possible to distinguish between the sectors via the phase φ of the Polyakov loop L

$$L(\mathbf{n}) = \frac{1}{3} \text{Tr}_C \left[\prod_{n_0=0}^{N_\tau-1} U_0(n_0, \mathbf{n}) \right] \equiv |L(\mathbf{n})| e^{i\varphi}. \quad (2.3)$$

Traversing the center sectors φ takes on the values $\langle \varphi \rangle = 2n\pi/3$, $n \in \mathbb{N}$. Hence measurements of the Polyakov loop and plotting its real versus its imaginary part yields scatter plots that resemble the three-armed arrow symbols in Fig. 1 (right). As indicated by the dotted lines the chiral/deconfinement transition analytically continues from $\mu = 0$ to imaginary chemical potential until it joins the RW transition in its endpoint. At this junction μ_i takes on the critical values $(\mu_i/T)_c$ and the phase structure in the $m_{u,d} - m_s$ plane, shown in Fig. 2 (right), is qualitatively different compared to zero chemical potential (c.f. Fig. 1). The nature of the chiral/deconfinement transition for $0 < \mu_i < (\mu_i/T)_c$ and of the RW endpoint is determined by the number of flavours and the values of the quark masses. Past studies [6, 4] for $N_f = 2, 3$ have found the RW endpoints to be first order triple points for heavy and low masses and second order endpoints for intermediate masses. This can be intuitively understood from drawing the Columbia plot with the chemical potential as an additional parameter (see Fig. 2). The $Z(2)$ critical lines of $\mu = 0$ become surfaces terminating in tricritical lines at imaginary chemical potential $(\mu_i/T)_c$ (the RW endpoints). Fixing in Fig. 2 the value of the quark masses and varying the chemical potential from $(\mu/T)^2 = 0$ to $-(\pi/3)^2$, as indicated by the arrow-headed vertical line, we move along the chiral/deconfinement transition line in the $T - \mu$ plane (Fig. 1 (right)). This line changes its nature from crossover to first

order with a second order point in between, joining the RW transition in its endpoint at $(\mu_i/T)_c$ rendering it a triple point. Depending on the mass the nature of the RW endpoint can be tricritical or second order $Z(2)$. Accordingly the chiral/deconfinement transition line can be first order or purely crossover.

3. Simulation details

The computational and algorithmic setup used for this work is similar to the former study about the RW transition on $N_\tau = 4$ lattices [6], i.e. with the standard Wilson gauge action and $N_f = 2$ flavors of unimproved Wilson fermions. The bare fermion mass $m_{u,d} \equiv m$ is indirectly controlled via the hopping parameter $\kappa = (2(am + 4))^{-1}$. The temperature $T = 1/a(\beta)N_\tau$ on the lattice is adjusted via change of the lattice coupling parameter β . For a fixed temporal lattice extent of $N_\tau = 6$ and imaginary chemical potential of $\mu_i/T = \pi$ we scanned for the tricritical points $\kappa_{\text{tric}}^{\text{light}}$ and $\kappa_{\text{tric}}^{\text{heavy}}$ in $\kappa \in (0.1, \dots, 0.165)$. For each value simulations at three to four different spatial lattice extents were done, where we kept $N_\sigma \geq 16$ except for $\kappa = 0.1625$ with $N_\sigma \geq 12$, which implies an aspect ratio of approximately three or larger in the most cases. For every spatial lattice extent the temperature scans included ~ 15 β values. The number of HMC trajectories (unit length) amounts to $\sim 40k - 500k$ per β value after at least $5k$ thermalization steps. In order to accumulate statistics faster the runs were distributed on four chains per β . This also helped to decide whether the statistics were large enough. Throughout all simulations the acceptance rate was tuned to $\sim 75\%$. For very small masses, i.e. $\kappa \geq 0.16$ the Hasenbusch trick [9] was applied in order to improve integrator stability. Our observables are the Polyakov loop and the chiral condensate which we measure on every trajectory. The simulations were performed with the OpenCL based code CL²QCD [10] which is highly optimized for running on graphic processing units (GPUs) on LOEWE-CSC[11] at Goethe University Frankfurt and on L-CSC[12] at GSI Darmstadt.

4. Analysis

We estimate the autocorrelation on the observables by a python implementation of the Wolff method [13]. An appropriate binning is then chosen in order to remove the autocorrelation effects in functions of the observables. In order to locate phase transitions and to extract their order we use the Binder cumulant

$$B_4(X, \alpha_1, \dots, \alpha_n) = \frac{\langle (X - \langle X \rangle)^4 \rangle}{(\langle (X - \langle X \rangle)^2 \rangle)^2}, \quad (4.1)$$

whose values which are listed in table 1 indicate the order of the phase transition. For $V \rightarrow \infty$ it is a non-analytic step function that depends on a set of parameters which are $\{\alpha_i\} = \{\beta, \mu_i^c\}$. We have chosen $X = L_{Im}$, where L is the spatial average of the Polyakov loop (c.f. Eq.(2.3)). On finite volumes B_4 gets smoothed out, passing continuously through the critical value, with its slope increasing with the spatial lattice extent. Close to the critical value of β , B_4 is a function of $x \equiv (\beta - \beta_c)N_\sigma^{1/\nu}$ solely and due to its scaling behaviour in the vicinity of a critical point can be expanded around 0 to leading order

$$B_4(\beta, N_\sigma) = B_4(\beta_c, \infty) + a_1x + a_2x^2 + \dots \quad (4.2)$$

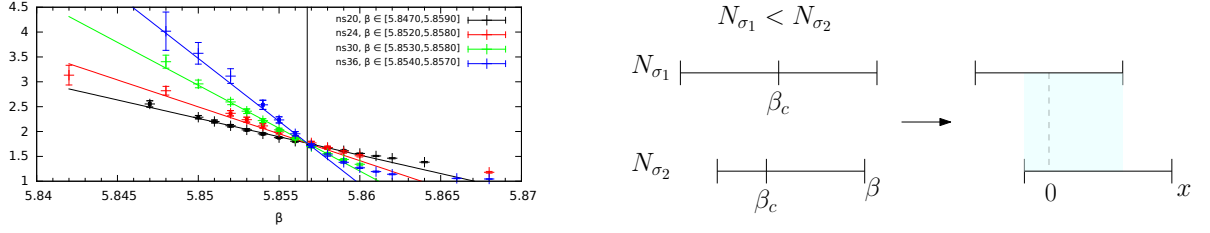


Figure 3: (Left) B_4 as function of imaginary chemical potential and N_σ at a fixed quark mass values. The different curves intersect at the critical value. (Right) Translation of the fitting ranges from β for different N_σ to the scaling variable $x = (\beta - \beta_c)N_\sigma^{1/\nu}$.

Varying the lattice coupling β we then measure B_4 at fixed μ_i along the phase boundary separating the RW sectors in the T -direction where the third moment of the fluctuations vanishes, $\langle (X - \langle X \rangle)^3 \rangle = 0$. This procedure is repeated for different spatial volumes each yielding a curve with a different slope. In order to smoothen the raw measurements and to fill in additional points Ferrenberg-Swendsen reweighting [14] was used. Subsequently a finite size scaling study is employed by fitting Eq.(4.2) to all data at once, as it is shown for an example in Fig. 3. The fitted value $B_4(\beta_c, \infty)$ is observed to be always larger than the values listed in Eq.(4.1)(right) which is in agreement with previous observations [15, 6] and can be explained by finite size effects not included in Eq.(4.2). A thorough investigation of this issue will be included in our future article [16]. Hence we concentrate on the critical exponent ν which is a better suited quantity since it is less prone to finite size effects. Close to a critical point it takes on its universal value depending on the universality class. The possible values are listed in table 1. Another important quantity is the susceptibility of the order parameter

$$\chi(X) \equiv N_\sigma^3 \langle (X - \langle X \rangle)^2 \rangle, \quad (4.3)$$

which as well scales around the critical value of β following

$$\chi = N_\sigma^{\gamma/\nu} f(tN_\sigma^{1/\nu}), \quad (4.4)$$

with a universal scaling function f and the reduced temperature $t \equiv (T - T_c)/T_c$. This can be used to check for consistency by plotting $\chi/N_\sigma^{\gamma/\nu}$ against $tN_\sigma^{1/\nu}$. All the different curves $\chi/N_\sigma^{\gamma/\nu}$ are supposed to collapse for a correctly determined value of ν . A further remark addresses the fitting procedure of Eq.(4.2) to the reweighted data $B_4(\beta_i, N_\sigma)$. Natural and straightforward criteria are

	Crossover	1 st triple	Tricritical	3D Ising
B_4	3	1.5	2	1.604
ν	—	1/3	1/2	0.6301(4)
γ	—	1	1	1.2372(5)

Table 1: Critical values of ν , γ and $B_4 \equiv B_4(X, \alpha_c)$ for some universality classes

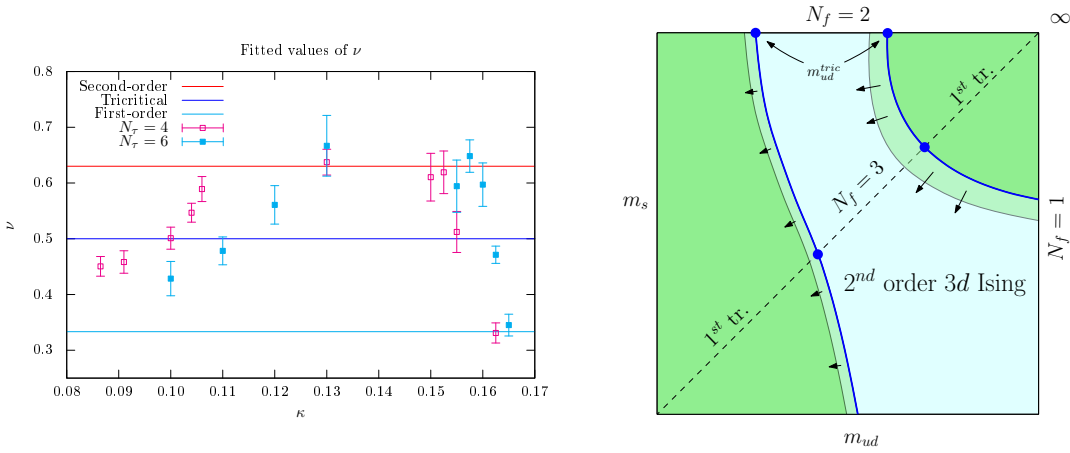


Figure 4: (Left) Results of the $N_\tau = 4, 6$ study combined in one plot. The $N_\tau = 6$ curve is shifted towards larger κ values. (Right) Schematic of the shift of the tricritical lines at μ_c^c/T to larger κ values.

$\chi^2 \approx 1$ and a goodness of the fit of $Q \approx 50$. Relying solely on these does not yet guarantee meaningful results as long as there is not a reasonable overlap in $x = (\beta - \beta_c)N_\sigma^{1/\nu}$ and an approximate symmetry in the fitting range around $x = 0$. The mapping from β to x is illustrated in Fig. 3. In order to respect these criteria we employ an algorithm which is repeating the fit for many combinations of β -ranges of the different curves (which again is coupled to certain boundary conditions) and filters amongst all the fits with proper χ^2 and Q the ones with the largest overlap in x and symmetry around $x = 0$. Again a detailed discussion about this will be included in our future article [16].

5. Numerical results

In the infinite volume limit the critical exponent is a step function of κ . This function is smeared out on finite volumes as indicated in Fig. 4 (left). For this reason the collapse plot technique does not provide meaningful results for the case when the critical exponent on the finite lattice is in between the values of table 1. Ultimately a further refinement is taken with the sophisticated fitting procedure briefly discussed in the previous section which allows for a more accurate resolution of the critical exponent ν in a rather quantitative way. We estimate the following two critical values of κ

$$\kappa_{\text{heavy}}^{\text{tric}} = 0.110(10) \quad \text{and} \quad \kappa_{\text{light}}^{\text{tric}} = 0.1625(25). \quad (5.1)$$

In Fig. 4 (left) we compare the results of this work to the former study [6] but for the sake of clarity we did not include all the data points of the $N_\tau = 4$ study. It appears that the $N_\tau = 6$ curve is shifted towards smaller mass values or a shift of the first order region towards lower mass values respectively as illustrated schematically in Fig. 4 (right).

6. Summary and Perspectives

QCD at imaginary chemical potential μ_i features many interesting properties which can be used to constrain the QCD phase diagram at real μ where it is not possible to apply standard

simulation algorithms due to the sign problem. Our study of the imaginary region at $\mu_i = \pi T$ on $N_\tau = 6$ lattices with unimproved Wilson fermions are consistent with the findings of former studies and we observed the expected shift of the tricritical masses to smaller values. Despite getting one step closer to the continuum it is still not possible to make a definite statement about the rate of the shift of κ_{tric} in dependence of the temporal lattice extent. It will be interesting to see the results of the future studies on higher N_τ lattices.

Acknowledgments

This work is supported by the Helmholtz International Center for FAIR within the LOEWE program of the State of Hesse. We thank the staff of LOEWE-CSC and L-CSC at GU-Frankfurt and the NIC in Jülich for computer time and support.

References

- [1] Y. Iwasaki, K. Kanaya, S. Kaya and T. Yoshie, Phys. Rev. Lett. **78**, 179 (1997) [hep-lat/9609022].
- [2] M. D’Elia, A. Di Giacomo and C. Pica, Phys. Rev. D **72**, 114510 (2005) [hep-lat/0503030].
G. Cossu, M. D’Elia, A. Di Giacomo and C. Pica, arXiv:0706.4470 [hep-lat].
C. Bonati, G. Cossu, M. D’Elia, A. Di Giacomo and C. Pica, PoS LATTICE **2008**, 204 (2008) [arXiv:0901.3231 [hep-lat]].
- [3] S. Ejiri *et al.*, Phys. Rev. D **80**, 094505 (2009) [arXiv:0909.5122 [hep-lat]].
- [4] C. Bonati, P. de Forcrand, M. D’Elia, O. Philipsen and F. Sanfilippo, Phys. Rev. D **90**, no. 7, 074030 (2014) [arXiv:1408.5086 [hep-lat]].
- [5] A. Roberge and N. Weiss, Nucl. Phys. B **275**, 734 (1986).
- [6] O. Philipsen and C. Pinke, Phys. Rev. D **89**, no. 9, 094504 (2014) [arXiv:1402.0838 [hep-lat]].
- [7] P. de Forcrand and O. Philipsen, Nucl. Phys. B **642**, 290 (2002) [hep-lat/0205016].
- [8] M. D’Elia and M. P. Lombardo, Phys. Rev. D **67**, 014505 (2003) [hep-lat/0209146].
- [9] M. Hasenbusch, Phys. Lett. B **519**, 177 (2001) [hep-lat/0107019].
- [10] M. Bach, V. Lindenstruth, O. Philipsen and C. Pinke, Comput. Phys. Commun. **184**, 2042 (2013) [arXiv:1209.5942 [hep-lat]].
- [11] M. Bach *et al.*, Computer Science - Research and Development 26 (2011)
- [12] D. Rohr, M. Bach, G. Neskovic, V. Lindenstruth, C. Pinke and O. Philipsen, High Performance Computing LNCS 9137 (2015)
- [13] U. Wolff [ALPHA Collaboration], Comput. Phys. Commun. **156**, 143 (2004) [Comput. Phys. Commun. **176**, 383 (2007)] [hep-lat/0306017].
- [14] A. M. Ferrenberg and R. H. Swendsen, Phys. Rev. Lett. **63** (1989) 1195.
- [15] P. de Forcrand and O. Philipsen, Phys. Rev. Lett. **105**, 152001 (2010) [arXiv:1004.3144 [hep-lat]].
- [16] F. Cuteri, C. Czaban, O. Philipsen, C. Pinke and A. Sciarra (in preparation)